Contents lists available at ScienceDirect

Petroleum Science

journal homepage: www.keaipublishing.com/en/journals/petroleum-science



Original Paper

Development of self-generated proppant based on modified lowdensity and low-viscosity epoxy resin and its evaluation



Jia-Cheng Fan a, *, Zhan-Qing Qu a, **, Tian-Kui Guo a, Ning Qi a, Ming Chen a, Jian Hou a, Ii-Iiang Ge ^a. Xiao-Oiang Liu ^b. Ii-Wei Wang ^a

- College of Petroleum Engineering, China University of Petroleum, Qingdao, 266580, Shandong, China
- ^b Beijing International Center for Gas Hydrate, School of Earth and Space Sciences, Peking University, Beijing, 100871, China

ARTICLE INFO

Article history Received 21 September 2021 Received in revised form 13 May 2022 Accepted 16 May 2022 Available online 27 May 2022

Edited by Yan-Hua Sun

Keywords: Low-viscosity and low-density epoxy resin Resin toughening Self-generated proppant Performance evaluation

ABSTRACT

Hydraulic fracturing is a critical technology for the economic development of unconventional oil and gas reservoirs. The main factor influencing fracture propping and reservoir stimulation effect is proppant performance. The increasing depth of fractured oil and gas reservoirs is causing growing difficulty in hydraulic fracturing. Moreover, the migration of conventional proppants within the fracture is always limited due to small fracture width and rigid proppant structure. Thus, proppants with good transportation capacity and fracture propping effects are needed. First, a novel self-generated proppant based on toughened low-viscosity and low-density epoxy resin was developed to satisfy this demand. Then, proppant performances were evaluated. Low-viscosity and low-density epoxy resin was generated when the thiol-ene click chemical reaction product of eugenol and 1-thioglycerol reacts with the epichlorohydrin. Then, the resin was toughened with graphite particles to increase its compressive strength from 50.8 to 72.1 MPa based on micro-cracking mechanism and crazing-nail anchor mechanism. The adduct of diethylene triamine and butyl glycidyl ether and the SiO2 nanoparticles were treated as the curing agent and emulsifier respectively to form the emulsion. The emulsion is transformed into solid particles of various sizes within a reservoir to prop the fracture. Evaluation shows good migration capacity of this self-generated proppant due to the low density of epoxy resin.

© 2022 The Authors, Publishing services by Elsevier B.V. on behalf of KeAi Communications Co. Ltd. This is an open access article under the CC BY-NC-ND license (http://creativecommons.org/licenses/by-nc-nd/

4.0/).

1. Introduction

Hydraulic fracturing has been extensively used in oil and gas reservoirs to stimulate wells and enhance oil and gas recovery. In fracturing, the proppants are injected into the reservoir to prevent fracture closure under in-situ stress and to create fracture conductivity (Guo et al., 2018). Currently, solid proppants such as quartz sand and ceramsite are applied in hydraulic fracturing. Those proppants have high density and are carried by high viscosity liquids, and their applications have many limitations. High viscosity liquids are usually achieved by adding thickening agent. Nevertheless, the thickening agent is always detained in the reservoir and causes damage to fracture conductivity (Liu et al., 2018). Then, high viscosity of the sand-carrier also leads to high flow resistance

within the pipeline, wellbore and fractures, increasing the sandcarrier injection difficulty. The high density of the solid proppant causes poor migration and fracture propping, especially in branched fractures and micro-fractures, and sand plugs tends to occur. This causes ineffective far-end reservoir stimulation and reduces recovery rate of oil and gas (Zhang C., et al., 2019). Injection of solid proppants also causes wear on the pipeline and wellbore, and injection of a large volume of proppants at a high rate and pump pressure proposes high requirements on the wellhead, fracturing equipment and pipe string (Guo et al., 2017). Currently, fractures are propped through staged proppant placement. The far-end and branched fractures are propped by small-sized particles, and major fractures and near-wellbore fractures by large-sized particles. Nevertheless, staged proppant placement cannot always work within small-width fractures created in deep and hard formations. Therefore, a self-generated proppant was developed, and its per-

Given the performance defects of conventional solid proppants

formances were evaluated (Jiang et al., 2019).

^{*} Corresponding author.

^{**} Corresponding author. E-mail addresses: 958652006@qq.com (J.-C. Fan), quzhq@upc.edu.cn (Z.-Q. Qu).

mentioned in the previous paragraph, this self-generated proppant that can be injected into the reservoir in the liquid phase has become the main development direction of the propping material. There are three types of self-generated proppants: small molecular gels, supramolecular polymers, and emulsified thermosetting epoxy resins. Small molecule gels refer to organic molecules with a molecular weight below 2000 that directly form structures with strength through non-covalent interaction between molecules when they are stimulated by the outside world. Supramolecular gel is a three-dimensional structure that is further entangled under the stimulation of external factors after the gelation of small molecules through non-covalent interaction. Emulsified thermosetting epoxy resins is an oil-in-water emulsion prepared by mixing the thermosetting epoxy resin with its curing agent and emulsifying them. The resin and curing agent in the droplets are cured under stimulation of reservoir temperature to obtain proppants with different particle sizes (Pei et al., 2021). Through literature research, the properties of the three kinds of self-generated proppants were analyzed. A novel self-propping fracturing fluid system was developed base on the gelatinization of the small molecule gel after heating. The phase change liquid (PCL) is carried by the non-phase change liquid (NPCL), injected into the reservoir, and transformed into solid particles in the reservoir above 85 °C. The generated particles have low density and high compressive strength, and particle size ranges from 20/40 mesh to 40/70 mesh and cannot be changed during the transformation process. Small molecule gels have leak-off in hyperpermeable reservoirs (Zhao et al., 2019). Phase change proppants, applicable in a reservoir temperature of 60-90 °C, were developed through liquid-solid phase change of supramolecular materials with increasing temperature. The effect of proppant generation in the reservoir environment was evaluated. Particles formed in the flowing state have uniform and smaller sizes, and those formed in the static state have larger and irregular sizes (Luo et al., 2019). One kind of self-generated proppant based on bisphenol-A epoxy resin is obtained with an emulsification method in the laboratory. Proppant sizes are mainly distributed in 30-50 mesh, and the proppants have good compressive strength and sphericity (Wang, 2020).

The morphology and particle size uniformity of proppant particles affect their performance. Therefore, the three kinds of selfgenerated proppants were optimized. The formation process of the self-generated proppant based on small molecule gels is uncontrollable, resulting in poor morphology uniformity of the obtained proppant particles. At the same time, when small molecular gels are used in a reservoir with high permeability, their effect reduces due to leak-off. The particle sizes of self-generated proppants based on supramolecular materials are uniform under stirring conditions, but the proppants particles obtained in the static state are larger and less uniform. Since the self-generated proppant is formed during standing after migrating into the reservoir, the obtained self-generated proppants based on supramolecular materials cannot meet the needs of efficient development. With mature emulsification technology, emulsion droplets usually have extremely high sphericity, and droplet sizes are controllable and can be changed by optimizing the emulsification process (Anton et al., 2008). Therefore, the emulsified thermosetting epoxy resin was selected to prepare self-generated proppants in this paper. Through investigation and preliminary evaluation experiments, it was found the high viscosity and high density of the epoxy resin make emulsion droplets prone to accumulation due to settlement during the transportation process. Accumulation can cause particle deformation, and droplets in the accumulation state are prone to coalesce between particles due to the increase of viscosity during the curing process. The poor toughness and notch-sensitive defects of epoxy resin can also decrease the compressive strength of the

obtained proppant particles (Zhang W., et al., 2019). In this study, a novel emulsified epoxy resin was used to develop self-generated proppants. First, low-viscosity and low-density epoxy resin was synthesized with monomers eugenol, epichlorohydrin and thioglycerol, eliminating poor emulsion migration and easy accumulation of particles (Ohki, 2010). Then, the generated epoxy resin was toughened to enhance the compressive strength of proppant particles, and self-generated proppants of different sizes were obtained through emulsification. Finally, the performances of the selfgenerated proppant were evaluated. Through the evaluation experiment, it was found the new self-generated proppant has better migration ability than traditional solid proppants due to its lower density and deformability of emulsion droplets, which have better support for distal fractures and micro-fractures. This new self-generated proppant can also be directly carried by the fracturing fluid to simplify the fracturing construction process and its performance can meet the requirements in applications of reservoir fracturing.

2. Development of the self-generated proppant

2.1. Materials

Dimethyl sulfoxide, 1-thioglycerol, eugenol, dimethylaminopyridine (DMAP, catalyst), epichlorohydrin (ECH) and sodium dodecyl benzene sulfonate (SDBS), which were obtained from Sinopharm Group Chemical Reagent Co., Ltd, (Shanghai, China), were used for synthesis of low-density and low-viscosity epoxy resin. Hydrophilic SiO₂ nanoparticles with a particle size of 50 nm (Zhongke Yanuo New Material Technology Co., Ltd., Beijing, China) and SDBS were used as emulsifiers. Elastic rubber, graphite and silica particles with an average size of 40 µm (Zhongke Yanuo New Material Technology Co., Ltd., Beijing, China) were used for toughening resins. Guar gum fracturing fluid (0.65% hydroxypropyl guar and 0.7% coumarin), quartz sand proppant and ceramsite proppant from Shengli Oilfield (Shandong, China) were used for evaluation of self-generated proppants.

2.2. Synthesis of the low-density and low-viscosity epoxy resin

Eugenol and 1-thioglycerol with a mole ratio of 1:1 and DMAP with a concentration of 2 wt% were dissolved in dimethyl sulfoxide, and stirred at 75 °C for 2 h until a light-yellow product was generated. Subsequently, the product reacted with ECH by adding an 10% sodium hydroxide ethanol solution and stirring the solution for 4 h at 95 °C (Fig. 1). Finally, the product was purified with an aqueous solution of sodium hydroxide to obtain the low-viscosity and low-density epoxy resin (Wan et al., 2012; Grishchuk and Karger-Kocsis, 2011; Jin et al., 2015). The obtained epoxy resin is colorless (Fig. 2), and the epoxy resin based on renewable eugenol was first applied as proppant material.

Fig. 1. Reaction formula of the low-density and low-viscosity epoxy resin.

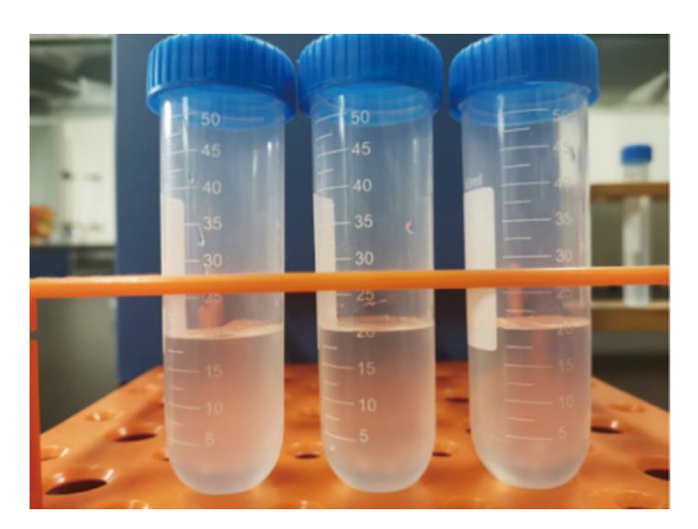


Fig. 2. Morphology of the low-density and low-viscosity epoxy resin.

2.3. Toughening of the low-density and low-viscosity epoxy resin

In order to resolve the poor toughness and notch sensitivity of epoxy resin, the generated low-density and low-viscosity epoxy resin was toughened with various materials. First, the optimum toughening material was determined (Ren, 2011), then the optimum concentration was determined and the resin toughening mechanism was analyzed.

2.3.1. Optimization of toughening materials

First, elastic rubber particles, graphite particles, and silica particles were respectively added to three groups of the generated resin, and the particle concentration was 4 wt%. Then, the resin viscosity was reduced by adding anhydrous ethanol as diluent, and stirred for 30 min at 300 rpm to mix the resin and toughening particles evenly. In this study, adduct of diethylene triamine and butyl glycidyl was used as curing agent. When the mass ratio of resin to curing agent is 4:1, the resin can be fully cured in a wet environment above 60 °C within 40 min. Finally, the compressive strength of the cured resin was tested in a triaxial compression device and the toughening effects were analyzed through SEM observation of particle morphologies.

The compressive strength of the cured epoxy resins toughened with elastic rubber particles, graphite particles and silica particles are shown in Fig. 3.

The compressive strength of the resin was improved after adding the elastic and rigid materials. Rigid particles toughened the epoxy resin better than elastic particles. The compressive strength of the resin toughened with elastic rubber increased from 50.8 to 60.3 MPa; and for the resins toughened with graphite particles and silica particles their compressive strength values increased to 72.1 and 73.5 MPa, respectively. The displacement of the resins toughened with graphite and silica particles under compression was 0.55 and 0.21 mm, respectively. The resin toughened with graphite had better toughness while its compressive strength was close to that of the resin toughened with silica particles (Kang et al., 2001). This is because graphite particles, which have a more spherical surface than silica particles (Fig. 4), can reduce particle agglomeration and are distributed more uniformly (Zhou et al., 2005). It can be judged the poor toughness and notch sensitivity of epoxy resin can be mitigated by adding graphite particles as the toughening material. Adding graphite particles to proppants, which support the fracture under high closure pressure, prevents blocking of tiny fractures caused by proppant crushing. Therefore, graphite particles were

selected as the toughening material for the resin in this study.

2.3.2. Optimization of the amount of the toughening material

Graphite particles with the concentration from 1 wt% to 7 wt% were added to the resin, and the compressive strength of the cured resin was evaluated. Through SEM observation of the end face of the crushed cured resin, the toughening mechanism of particle materials and the effects of various material concentrations were obtained. The compressive strength of the low-viscosity and low-density epoxy resin toughened with graphite particles of different concentrations is shown in Fig. 5.

When the graphite particle concentration was less than 5 wt%, the compressive strength of the toughened resin increased with an increase in particle concentration. When the graphite particle concentration increased from 0 to 5 wt%, the compressive strength of the toughened resin increased from 50.8 to 74.0 MPa. Nevertheless, as the graphite particle concentration continued to increase, the compressive strength of the toughened resin decreased. When the concentration of graphite particle increased to 7 wt%, the compressive strength of the toughened resin reduced to 70.3 MPa due to excessive particle accumulation. According to Fig. 6, lowconcentration graphite particles are distributed uniformly within the resin. Thus, graphite particles can restrict resin deformation by mitigating the movement of the adjacent resin matrix (Jiang et al., 2018). An increase in graphite particle concentration causes agglomeration and small cavities within the resin due to poor wettability of graphite and epoxy resin and the irregular morphology of graphite particles (Guo L., et al., 2012). Thus, the concentration of graphite particles in toughening the low-viscosity and low-density epoxy resin should be less than 5 wt%, and the optimum value is 3 wt% in this study.

2.3.3. Mechanism of toughening low-viscosity and low-density resin

According to the micromorphology of the end surface of cured low-viscosity and low-density epoxy resin (Fig. 7), the resin is toughened by graphite particles through various mechanisms. First is the micro-crack mechanism (Fig. 7a). Based on this theory, the main crack is generated during fracture propagation, and secondary cracks are generated when encountering rigid particles (Chen and Chang, 2001). New secondary cracks need to absorb more energy to expand, and this process effectively consumes the energy on the main crack and enhances the compressive strength of the resin material (Francis et al., 2006). Second is the crazing-nail anchor mechanism (Fig. 7b). This mechanism means that rigid particles are embedded on the fracture surface in the epoxy resin matrix, which prevents crazing extension caused by stress (Keller et al., 2017). At the same time, due to the formation of cavities after the toughening particles fall off, the energy consumed by deformation of the cavities is much higher than that consumed by matrix deformation, thereby enhancing the material strength.

2.4. Development of the self-generated proppant

The toughened low-density and low-viscosity epoxy resin and curing system are emulsified to form stable droplets dispersed in the fracturing fluid, and the particles are formed after droplets are solidified and support the fractures effectively.

2.4.1. Optimization of emulsifiers

With toughened epoxy resin, self-generated proppants are obtained through emulsification. In this study, SDBS (anionic surfactant) and hydrophilic SiO_2 nanoparticles at a concentration of 1 wt% were chosen as emulsifiers. The emulsification was carried out with the oil-water ratio of 1:5 by adding ethanol as diluent and stirring it

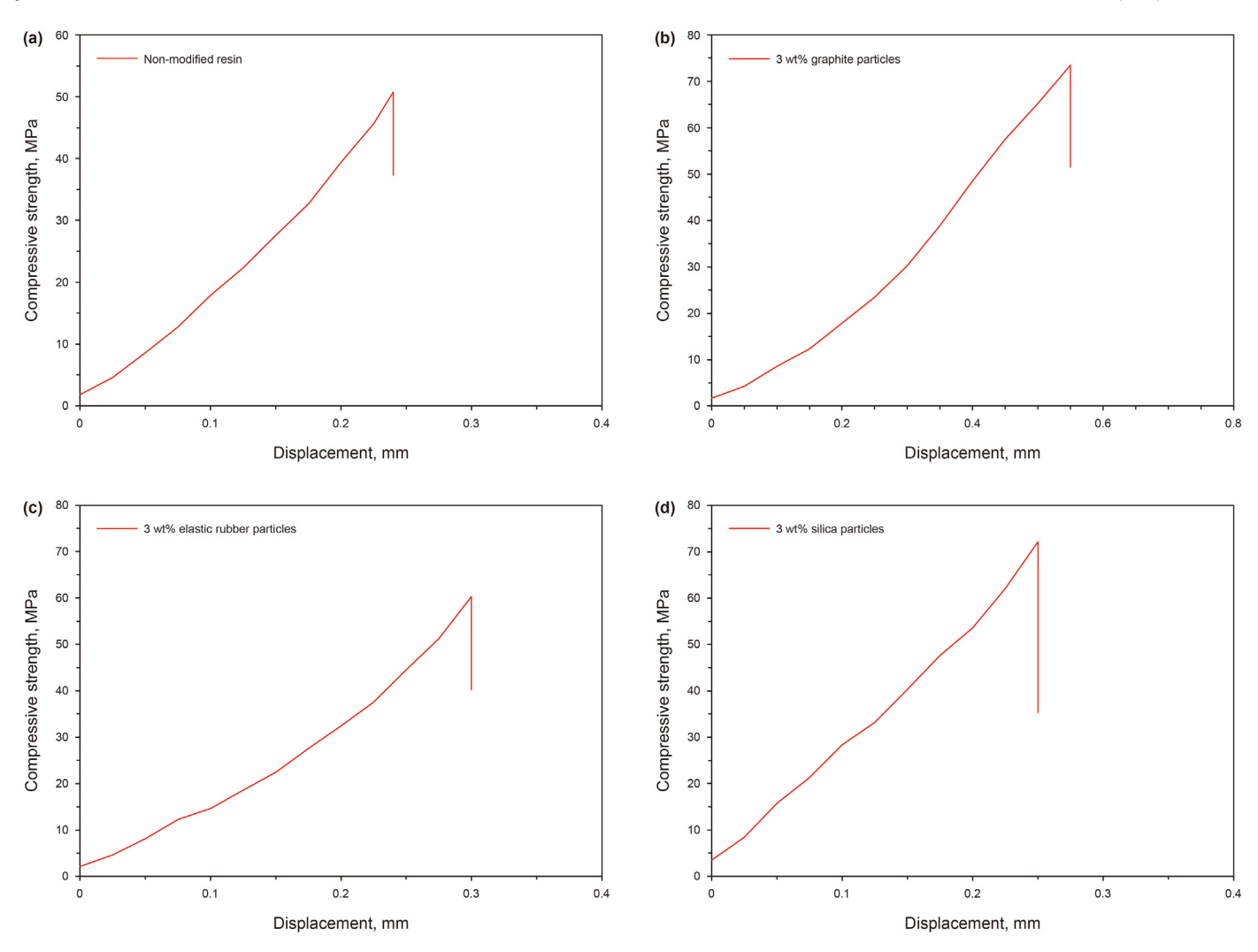


Fig. 3. Compressive strength of pure resin (a) and resins toughened with graphite particles (b), elastic rubber particles (c) and silica particles (d), respectively.

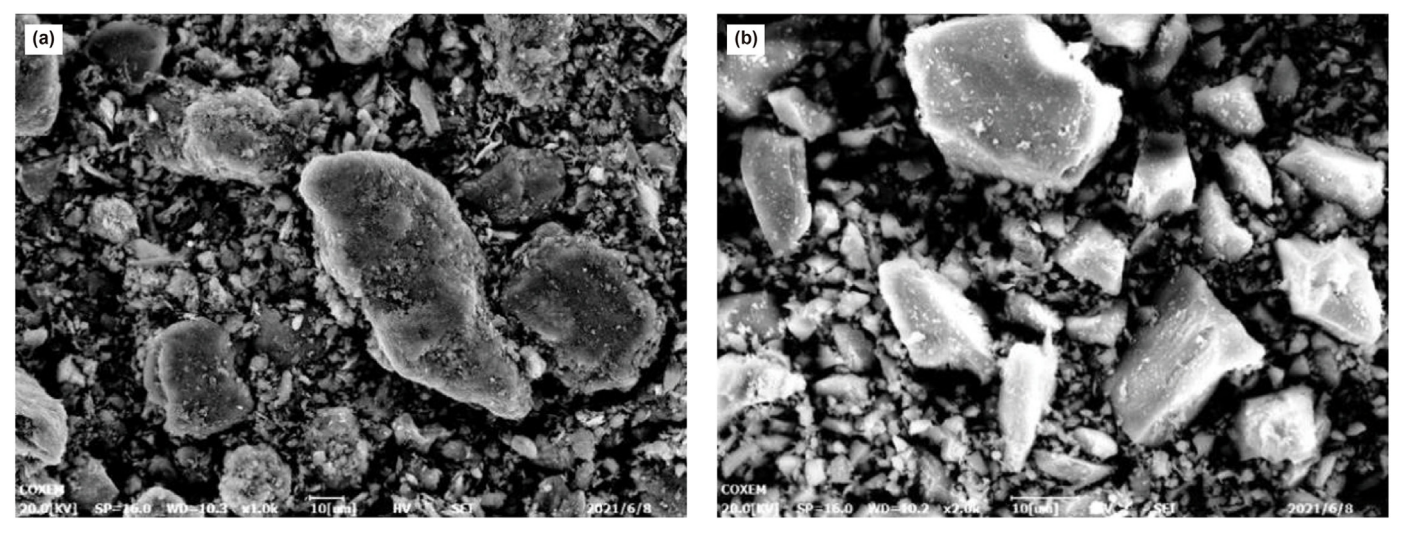


Fig. 4. Morphology of graphite particles (a) and silicon particles (b).

for 20 min at 300 rpm. The generated emulsion was kept static until the resin was cured. The morphology and microscopic surface of

the solidified proppants were observed through SEM to determine the optimum emulsifier, as shown in Figs. 8 and 9.

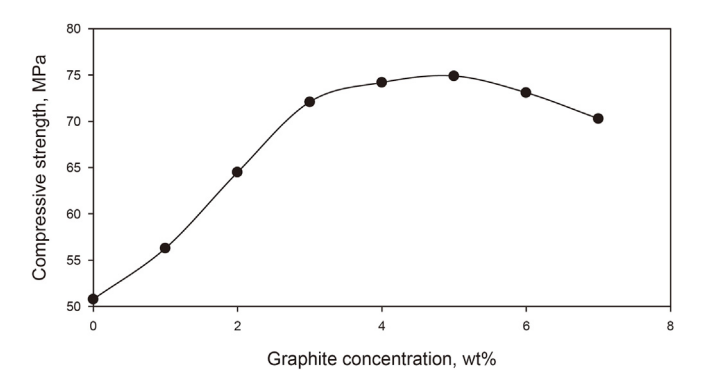


Fig. 5. Compressive strength of the low-viscosity and low-density epoxy resin toughened with graphite particles of different concentrations.

According to Figs. 8 and 9, proppants generated with SiO₂ nanoparticles as emulsifier had a relatively regular structure and larger size. The proppants generated with SDBS as emulsifier had a smaller size and poor regularity, and the particles adhered together. This is because adsorption of the active emulsifier at the oil-water interface is reversible, and a stable emulsion is formed through dynamic equilibrium of adsorption and desorption. The equilibrium is destroyed during curing of the resin due to the rising viscosity of the resin and this leads to irregular shapes of proppant particles (Ritzenthaler et al., 2002). Compared with the active

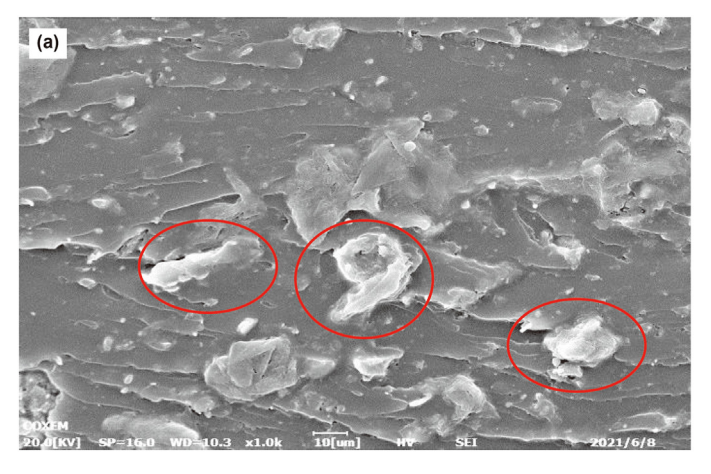
emulsifier, SiO_2 nanoparticles act as a mechanical barrier through irreversible adsorption at the oil-water interface. The barrier can prevent emulsion droplets from coalescing during the curing process (Haaj et al., 2014). Thus, the solid particles, SiO_2 nanoparticles, were selected as the emulsifier to generate the epoxy resin emulsion.

2.4.2. Optimization of emulsifier concentration

With the optimized emulsifier, the emulsification experiment was carried out with emulsifier concentration of 0.3 wt%, 0.5 wt%, 0.7 wt%, and 1 wt%, respectively. The emulsion was solidified to generate the proppants which were filtered with screens and weighed to determine particle size distribution.

When the concentration of SiO_2 nanoparticle is 0.5 wt%, the proppants with sizes >2.9 mm (7 mesh), 1.7–2.8 mm (7/12 mesh), 0.85–1.4 mm (14/20 mesh), 0.6–0.710 mm (25/30 mesh), 0.25–0.5 mm (35/60 mesh) and <0.18 mm (80 mesh) were generated. The size of the obtained proppant can meet the requirements of propping fractures in the near-wellbore area, major fractures and branched fractures at the same time. The size distribution of proppants changes with emulsifier concentration, and the size distribution of proppants obtained by SiO_2 nanoparticles of different concentrations were analyzed, as shown in Fig. 10.

The average size of the generated proppants decreases with an increase in emulsifier concentration. For example, when the concentration of SiO_2 nanoparticles is 0.3 wt%, the 7/12 mesh



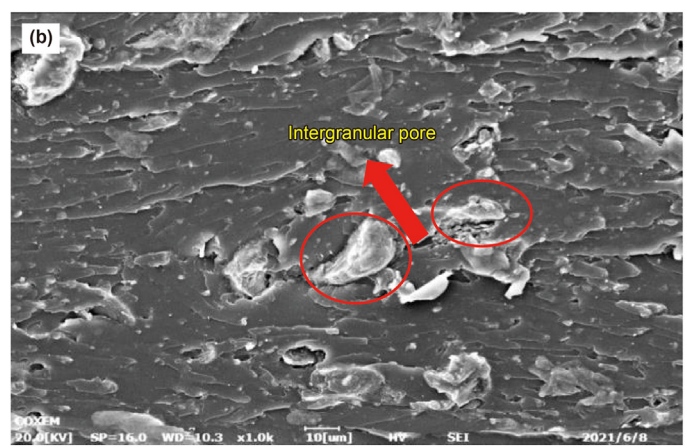


Fig. 6. Structures of resins toughened with graphite particles of different concentrations: (a) 5 wt%; (b) 7 wt%.

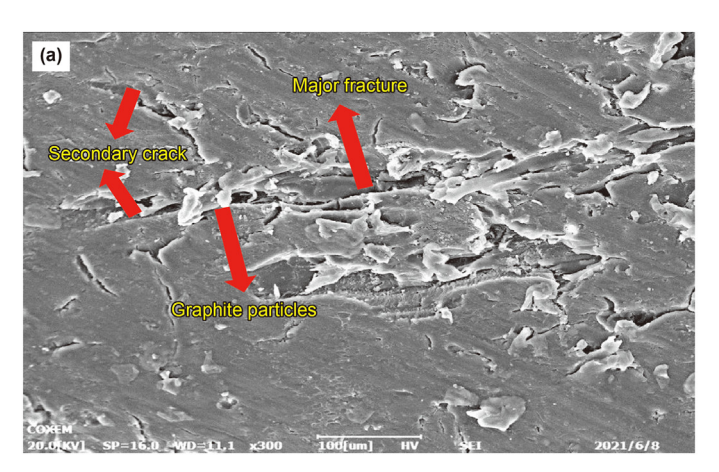
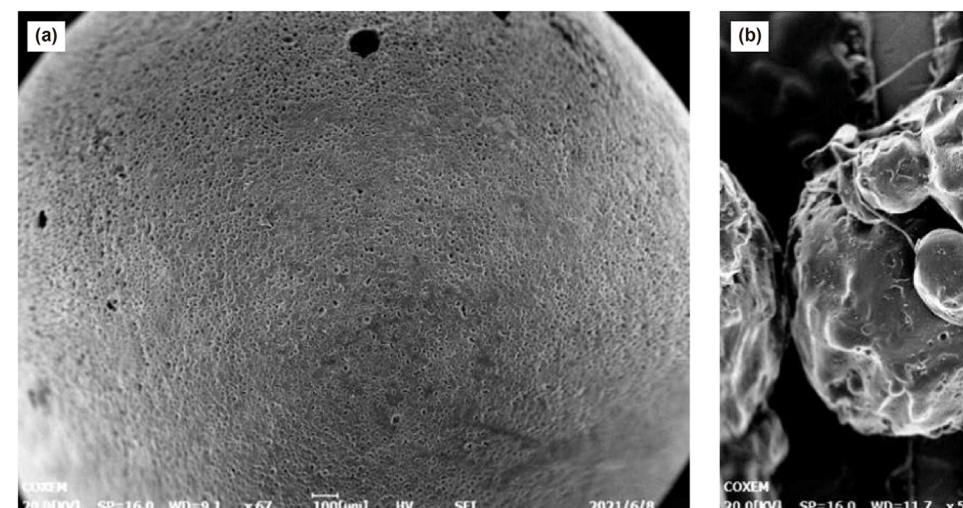




Fig. 7. Toughening mechanism of graphite particles.



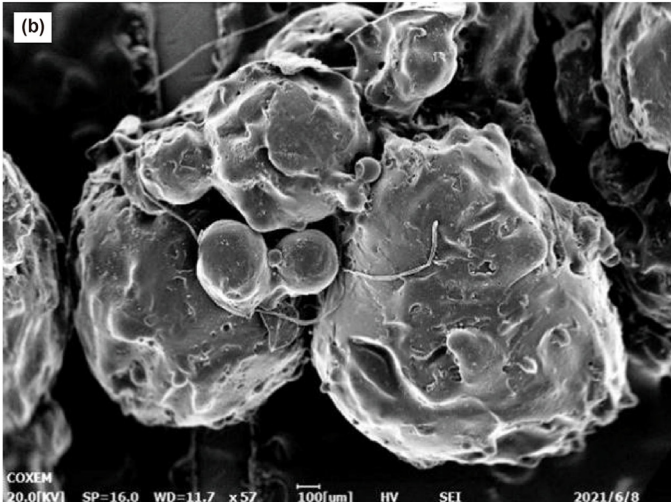
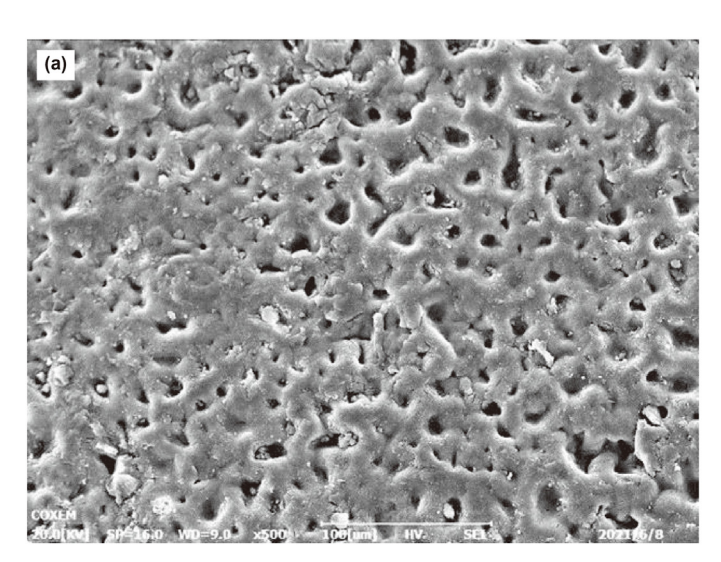


Fig. 8. Structures of proppant particles formed by different emulsifiers: (a) SiO₂ nanoparticles; (b) SDBS.



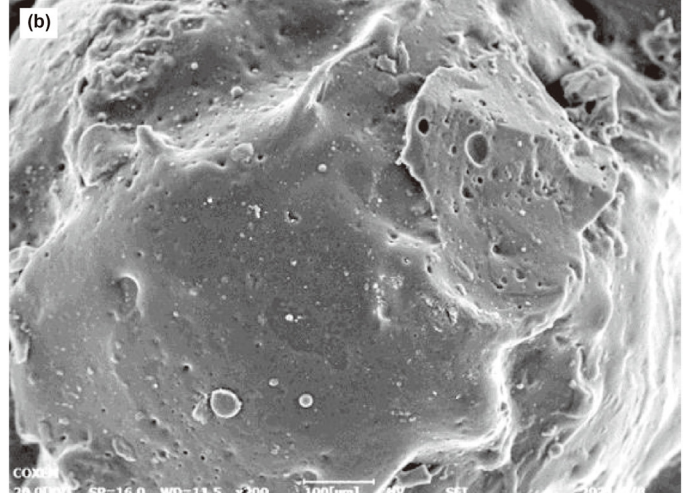


Fig. 9. Microscopic surface of proppant particles formed by different emulsifiers: (a) SiO₂ nanoparticles; (b) SDBS.

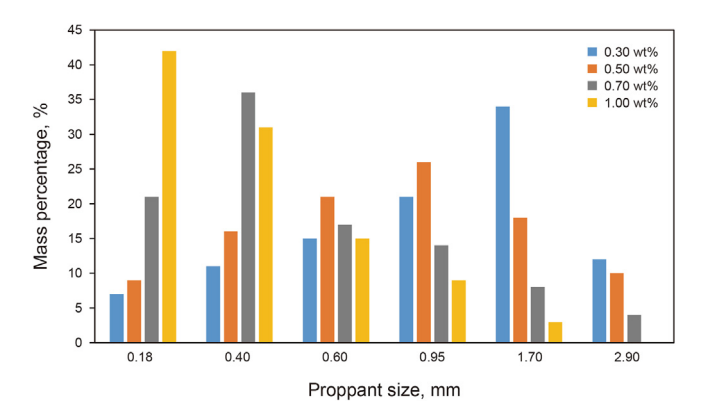


Fig. 10. Size distribution of proppants obtained by ${\rm SiO}_2$ nanoparticles of different concentrations.

proppants have the largest proportion in the generated proppants; when the emulsifier concentration rises to 0.7 wt%, the 35/60 mesh proppants have the largest proportion; when the emulsifier

concentration is 1 wt%, the proppants with the size <80 mesh have the largest proportion. In actual application, proppants with different size ratios can be obtained by changing the emulsifier concentration according to field requirements.

2.4.3. Optimization of oil-water ratio

The emulsifier concentration of 0.5 wt% was selected, and the oil-water ratio was optimized by evaluating emulsion stability with degree of creaming. The stability of the emulsion-phase self-generated proppant was evaluated at 800 rpm. The centrifugal force generated by this speed is much higher than that during the preparation and injection process of the on-site fracturing fluid (Guo T., et al., 2012). Then emulsions with oil-water ratios of 1:4, 1:5, 1:6 and 1:7 were prepared, respectively, and the obtained emulsions were centrifuged at 800 rpm for 20 min using a high-speed centrifuge. The oil-water ratio is optimized by evaluating the degree of creaming and the particle size distribution of cured proppants (Zhao et al., 2021). The experimental results are shown in Figs. 11—13 and Table 1.

$$D = \frac{V_{\text{oil}}}{V_{\text{t}}} \times 100\% \tag{1}$$

where D is the degree of creaming; V_{oil} is the volume of the separated oil phase, mL; V_{t} is the total volume of the emulsion, mL.

Evaluation results show the volume of the oil phase separated after centrifugation are 31.1%, 19.6%, 9.3%, and 6.8% of the total oil phase volume for the emulsions with oil-water ratios of 1:4, 1:5, 1:6, and 1:7, respectively. When the oil-water ratio drops below 1:6, the volume fraction of the separated oil phase in the total oil phase drops below 10%, indicating that the emulsion formed with silica nanoparticles as an emulsifier has good stability. Emulsion stability increases with decreasing oil-water ratio because droplets are more likely to coalesce due to contact during high-speed centrifugation when the droplet concentration increase. As can be seen from the evaluation results, the mass percentage of largeparticle-size proppants in the obtained proppants increases with an increase in oil-water ratio. When the oil-water ratio is reduced to 1:6, the size distribution of cured proppant particles obtained after centrifugation is close to proppants without centrifugation. This shows that the obtained self-generated proppant has better stability, and the proppant particle size has good uniformity after injection into the reservoir. Therefore, the oil-water ratio of the prepared emulsion is set to 1:6.

3. Evaluation of the low-viscosity and low-density epoxy resin and the self-generated proppant

3.1. Evaluation of the low-viscosity and low-density epoxy resin

3.1.1. Viscosity and density

The viscosity of the obtained epoxy resin was evaluated at 20, 40, 60, and 80 $^{\circ}$ C with an Anton Paar rheometer at a shear rate of 30 s⁻¹. Then, density was obtained by measuring the mass of the epoxy resin per unit volume.

3.1.2. Calculation of epoxy value

Epoxy value is the amount of epoxy groups in 100 g epoxy resin. The epoxy value of the obtained epoxy resin was determined with the hydrochloric acid-acetone method (Gaina and Gaina, 2009):

$$E = \frac{(V_0 - V)C}{10m} \tag{2}$$

where V is the volume of NaOH solution consumed by the sample, mL; V_0 is the volume of NaOH solution consumed by the blank sample, mL; C is the NaOH concentration, mol/L; m is the sample mass, g.

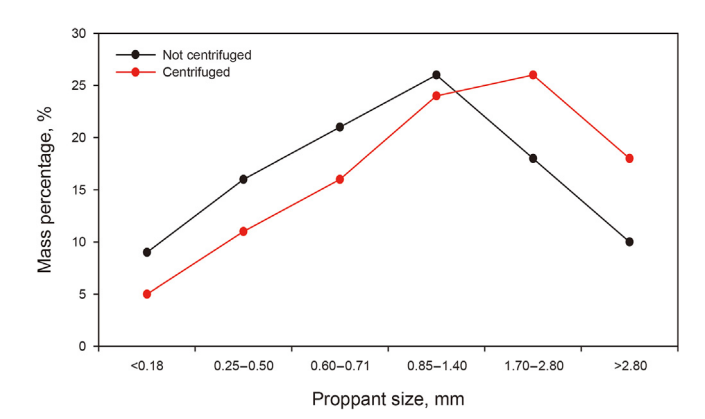


Fig. 12. Particle size distribution of proppants obtained by oil-water ratio of 1:5 before and after centrifugation.

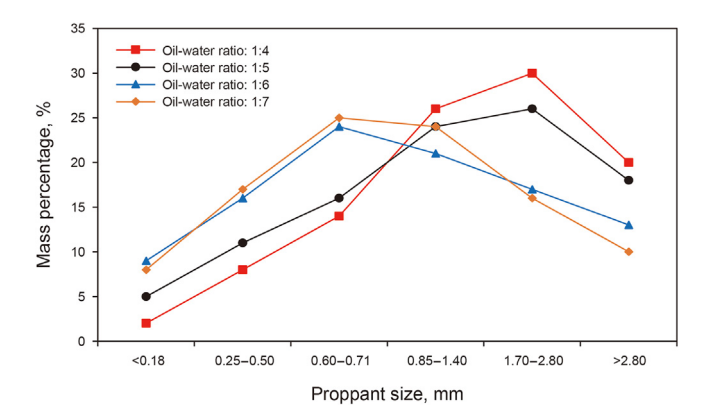


Fig. 13. Particle size distribution of proppants obtained by different oil-water ratios.

 Table 1

 Degree of creaming of emulsions with different oil-water ratios.

Oil to water ratio	Volume fraction of oil phase, %	Degree of creaming, %
1:4	16.7	5.2
1:5	13.8	2.7
1:6	11.8	1.1
1:7	10.3	0.7

3.2. Evaluation of the self-generated proppant

For self-generated proppants based on modified low-viscosity and low-density epoxy resin, the settlement and migration of the emulsion and permeability of the proppant pack were evaluated, respectively, to determine its performance and applicable reservoir

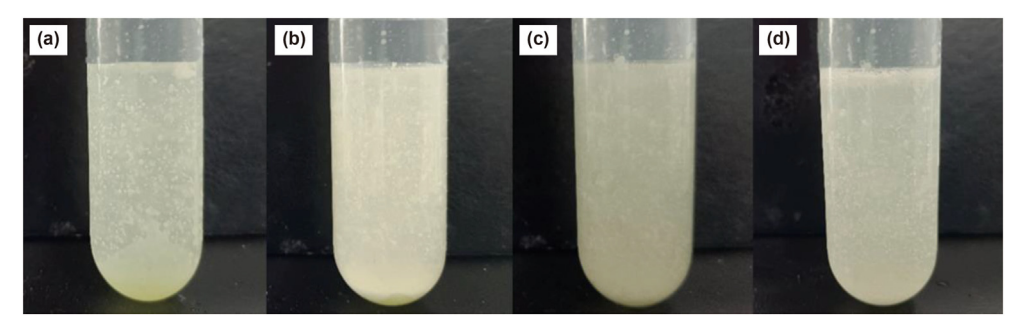


Fig. 11. Results of entrifugation experiments of emulsions with oil-water ratios of 1:4 (a), 1:5 (b), 1:6 (c) and 1:7 (d), respectively.

(Rui et al., 2018).

3.2.1. Migration capability

The proppant migration experiment was carried out in the visual proppant sedimentation and transportation device (Fig. 14) with guar gum fracturing fluid as the sand carrier. The migration capability of the self-generated proppants and quartz sand proppants of the same size in fracturing fluids of various viscosities were evaluated and compared. The experimental scheme is shown in Table 2.

3.2.2. Simulation of proppant migration

COMSOL Version 5.5 was used to establish a model for simulation of proppant migration to evaluate the migration capability of the self-generated proppant within a real fracture. The fluid carries the model's emulsion droplets of different sizes, and momentum exchange occurs between the droplets and the fluid. Thus, the droplets have a certain flow rate. The droplets also have a downward acceleration under the action of gravity and viscous resistance. The droplets of various sizes are subject to different gravity and viscous resistance, leading to different states of sedimentation and horizontal migration (Li et al., 2016).

(1) Assumptions

For the dispersed phase, only the effects of gravity and viscous forces were considered. Furthermore, the model at a constant temperature does not involve energy exchange: particle sedimentation follows the Navier-Stokes law (Hu et al., 2018).

(2) Governing equations

The motion equation of the dispersed phase can be expressed as (Rao et al., 2002):

$$\frac{\partial \varphi}{\partial t} + \nabla \cdot (\varphi v) = -\frac{\nabla \cdot J_{S}}{\rho_{S}} \tag{3}$$

where φ is the volume fraction of the emulsion droplet, %; v is the suspension velocity, m/s; J_s is the particle flux; ρ_s is the emulsion droplet density, kg/m³.

Navier-Stokes equations are expressed as (Adnan et al., 2021):

$$\frac{J_{\rm S}}{\rho_{\rm S}} = -\left[\varphi D_{\varphi} \nabla (\dot{\gamma}\varphi) + \varphi^2 \dot{\gamma} D_{\eta} \nabla (\ln \mu)\right] + f_{\rm h} \nu_{\rm St} \varphi \tag{4}$$

where $\dot{\gamma}$ is the shear rate tensor, s⁻¹; μ is the dynamic viscosity, mPa s; $f_{\rm h}$ is the settlement resistance, N; $v_{\rm st}$ is the settling velocity of a single particle surrounded by a fluid, m/s; D_{φ} and D_{η} are empirical fitting parameters and can be calculated by Eqs. (5) and (6):



Fig. 14. Visual proppant sedimentation and transportation device.

$$D_{\varphi} = 0.41a^2 \tag{5}$$

$$D_n = 0.62a^2 \tag{6}$$

where *a* is the radius of particles, m.

The shear rate tensor and the particle settling velocity are related to the velocity field. Therefore, the motion equation of the dispersed phase and Navier-Stokes equations are coupled through the velocity field.

(3) Initial and boundary conditions

The model boundary follows Dirichlet conditions. Left and right boundaries are the inlet and the outlet. For other boundaries, there are no inflow or outflow for fluids and particles. The entire model is filled with a continuous phase which flows at inlet flow rate. The dispersed phase is carried by the fluid from the inlet and flows out from the outlet. The initial value of the velocity field is 0. The key boundary conditions are marked in Fig. 15.

(4) Simulation meshes and computation time settings

Meshing uses a triangular level refinement mesh. The mesh number is 28,620, the mesh vertices are 14,737, the edge elements are 852, and the mesh area is 7,200,000 mm². The time step for the computation settings is 0.1 s, and the calculation time is 20 s.

(5) Simulation parameters

The specific parameters for simulation of migration capability of the self-generated proppants of five sizes are listed in Table 3.

3.2.3. Permeability of solidified proppant packs

The pack permeability of 40/70 mesh self-generated proppant, ceramsite proppant, and quartz sand proppant under closure stress were evaluated using a high-temperature hydraulic fracturing and seepage simulation device (Fig. 16). Proppant morphology was observed. The device can be operated under a confining pressure of up to 60 MPa. The test process is as follows:

- (1) Place different types of proppants in a single layer in the core to form proppant-filled fracture (Fig. 17);
- Hold the core in the core holder and place it in the hightemperature seepage simulation device;
- (3) Measure the permeability of proppant-filled fracture under closure stress of 5–50 MPa and at 40, 60, and 90 °C.

4. Results and discussion

4.1. Physical properties of low-viscosity and low-density epoxy resin

4.1.1. Viscosity and density

The density and viscosity of the obtained epoxy resin are shown in Table 4.

The viscosity of the epoxy resin generated in this study is 4620 mPa s at 20 °C, much lower than the bisphenol A epoxy resin (11,000 mPa s). Viscosity of epoxy resin is very sensitive to temperature. When the temperature rises above 60 °C, its viscosity drops to 686 mPa s. The density of the obtained epoxy resin remains constant at 1.2 g/cm³, lower than the conventional epoxy resins (1.6–2.3 g/cm³) and the traditional solid proppants (quartz sand: 2.2–2.3 g/cm³, ceramsite: 1.7–1.9 g/cm³). This is because the

 Table 2

 Experimental scheme of migration and settlement experiments.

No.	Proppant types	Injection rate, m ³ /h	Proppant concentration, %	Fluid viscosity, mPa s
1	Quartz sand Self-generated proppant	5.4	10	1
2	Quartz sand Self-generated proppant	5.4	10	15
3	Quartz sand Self-generated proppant	5.4	10	25

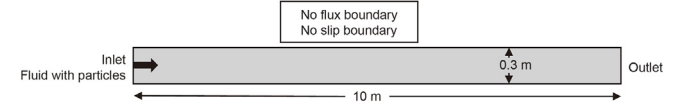


Fig. 15. Schematic diagram of key boundary conditions.

Table 3 Simulation parameters.

Parameter name	Numerical value
Inlet flow rate, m/s	0.1
Frac fluid density, kg/m ³	1
Self-generated proppant density, kg/m ³	1.2
Frac fluid viscosity, mPa s	1
Mass fraction of particles, %	14.3
Volume fraction of particles, %	12.2
Type of proppant particle size, mm	0.18-2.9

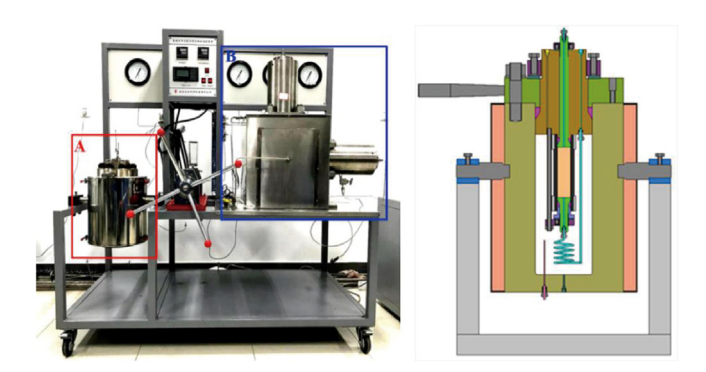


Fig. 16. High-temperature hydraulic fracturing and seepage simulation device.

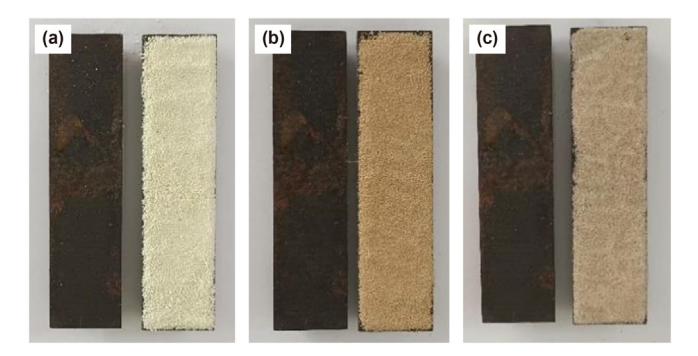


Fig. 17. Samples of self-generated proppants (a), ceramsite (b) and quartz sand (c).

molecular structure of the obtained epoxy resin has branched chains. The branched chains change the state of molecular chains stacking, decreasing the density and viscosity of the epoxy resin (Groenzin et al., 1999). The emulsion is easily generated due to the

Table 4Viscosity and density of the epoxy resin generated at different temperatures.

No.	Temperature, °C	Viscosity, mPa s	Density, g/cm ³
1	20	4620	1.2
2	40	1625	1.2
3	60	686	1.2
4	80	428	1.2

low viscosity of the resin. Epoxy resin with low density is suspended easily and has good migration ability in the frac fluid.

4.1.2. Epoxy value

The epoxy value of the low-viscosity and low-density epoxy resin is calculated to be 0.53 g/Eq, a high epoxy value. Therefore, less curing agent is required during the curing process, with lower application costs. High epoxy value also indicates that the cured resin has a higher hardness (Park et al., 2005).

4.2. Proppant settlement and migration

4.2.1. Experimental results

The results of the proppant migration experiments are shown in Figs. 18 and 19. Self-generated proppants have good migration capability compared with quartz sand proppants. There is difficulty in carrying quartz sand proppant with low viscosity fracturing fluid. When the fracturing fluid viscosity was 1 mPa s, the quartz sand proppants almost completely settled in the near-wellbore area and the front end of the main fracture. Self-generated proppants with particle size of 1.7–2.9 mm (>7 mesh and 7/12 mesh) settled rapidly in the near-wellbore area, and the 0.6–1.4 mm (14/ 20 mesh, 25/30 mesh and 35/60 mesh) self-generated proppants settled to prop the major fracture. Self-generated proppants with sizes <0.5 mm (<60 mesh) did not settle, indicating they can be carried by the low-viscosity fracturing fluid. Small proppant particles can prop far-end fractures and branched fractures. Rapid settlement of the larger proppants can prevent tiny cracks from plugging. When the fracturing fluid viscosity increased to 15 and 25 mPa s, the migration capability of quartz sand proppants was improved. Nevertheless, many quartz sand proppants still settled within the major fracture and cannot be carried to far end fractures. When the fracturing fluid viscosity was 15 mPa s, the self-generated proppant that settled in the near-wellbore area was reduced significantly and the proppants with sizes >7 mesh, 7/12 mesh and 14/20 mesh can be carried to far-end fractures. When the fracturing fluid viscosity increased to 25 mPa s, self-generated proppants did not settle significantly. That means the placement of self-generated proppants can be adjusted by controlling the fracturing fluid viscosity.

4.2.2. Simulation results

Experimental results in Fig. 18 are compared with the simulation results in Fig. 20. Simulation results are consistent with experimental results, proving the model has good accuracy. Since

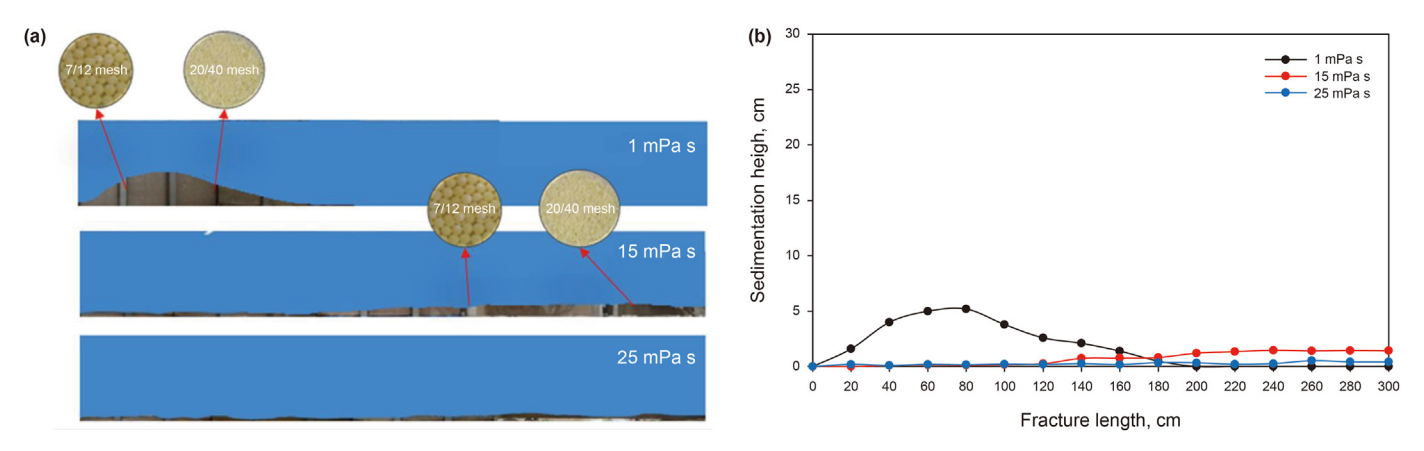


Fig. 18. Migration and settlement experiment results of self-generated proppants: (a) experimental picture, (b) height of the deposited sand bank.

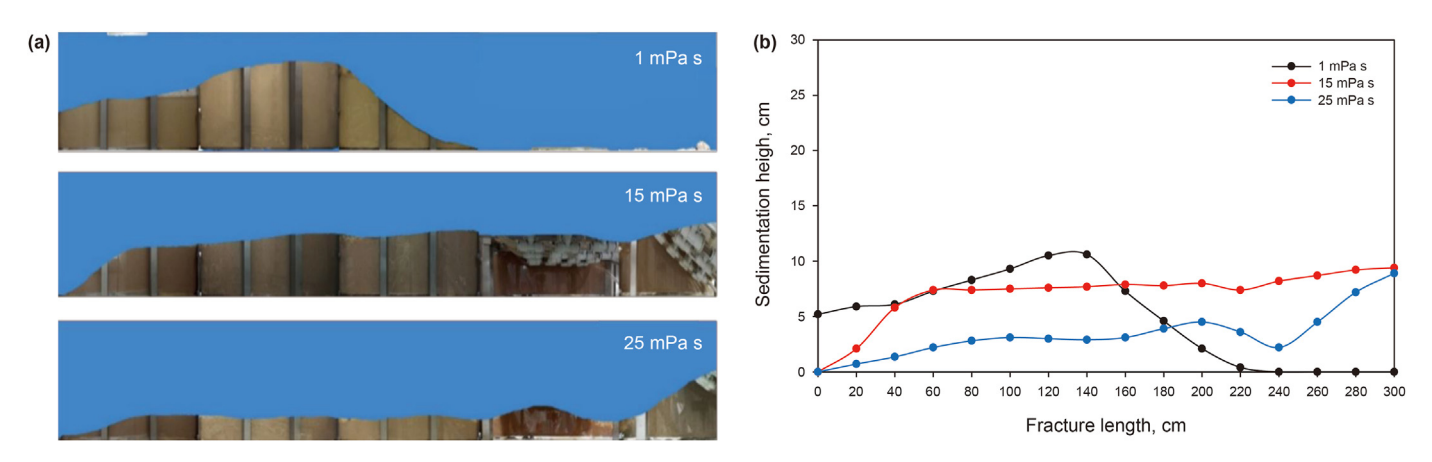


Fig. 19. Migration and settlement experiment results of quartz sand proppants: (a) experimental picture, (b) height of the deposited sand bank.

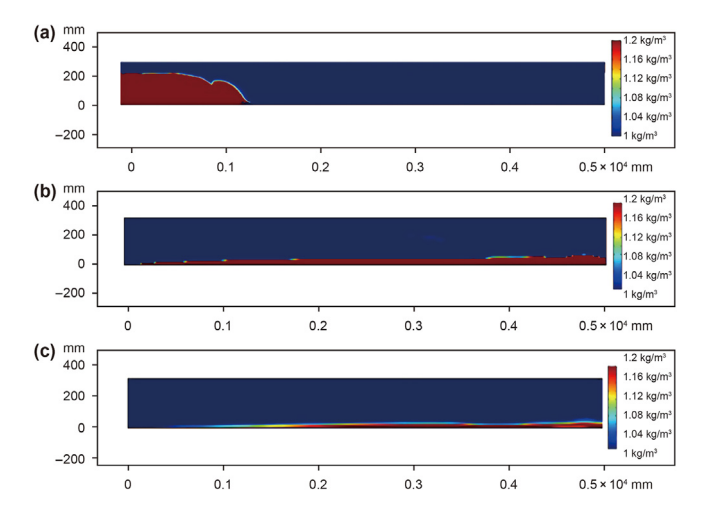


Fig. 20. Settlement and migration morphology of self-generated proppants with sizes of 0.18–2.9 mm in carrier fluids of different viscosities. (**a**) 1 mPa s, (**b**)15 mPa s, (**c**) 25 mPa s.

the initial flow rate of the proppant and fracturing fluid at the inlet of the experimental device differs from the uniform inflow in simulation, the proppants hardly settled at the inlet, leading to the differences in its sedimentation morphology.

The model was expanded to simulate migration and settlement of proppants within fractures close to real size. Finally, a 10 m long

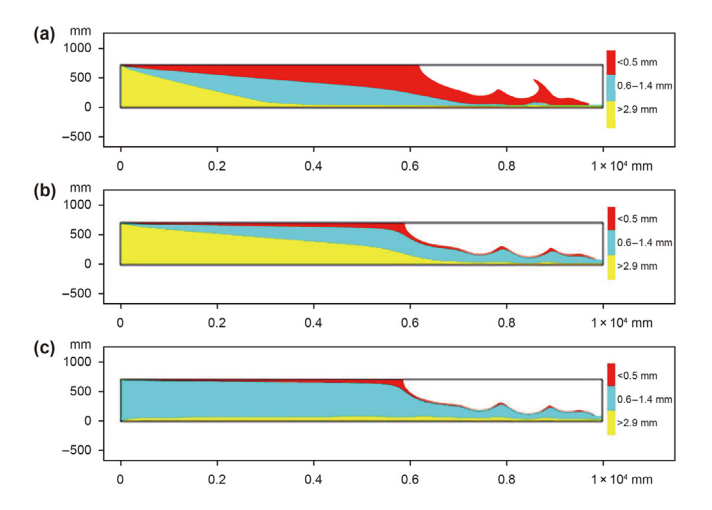


Fig. 21. Settlement and migration morphology of proppants with different sizes in fractures close to real size and in sand carriers of different viscosities. (**a**) 1 mPa s; (**b**) 15 mPa s; (**c**) 25 mPa s.

fracture model was established to simulate settlement and migration of proppants of different sizes in a sand carrier of various viscosities.

Simulation results are shown in Fig. 21. Colors correspond to proppants with different particle sizes. When the color is full of fractures, it means the type of proppant particle size represented by

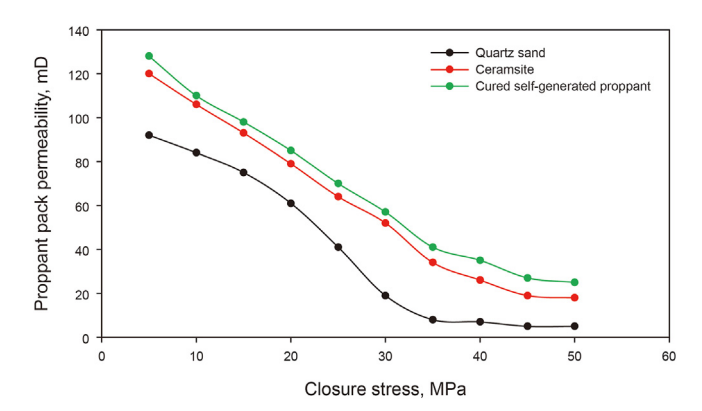


Fig. 22. Proppant pack permeability under different closure stresses.

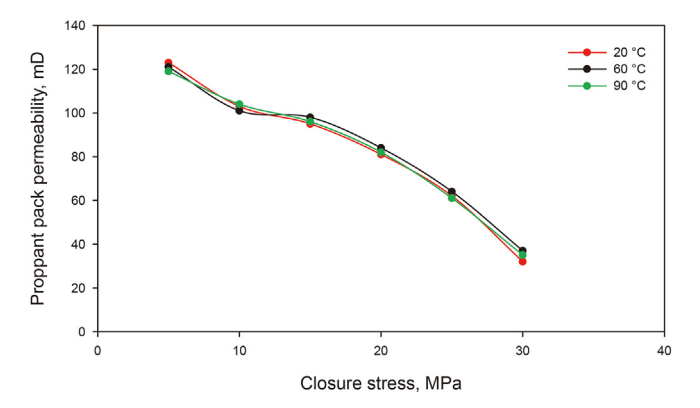


Fig. 23. Pack permeability of self-generated proppants at different temperatures.

this color is effectively carried. When the color corresponding to the proppant appears on a downward slope, it indicates it has begun to

settle. When the fracturing fluid viscosity is 1 mPa s, proppants with sizes of 1.7–2.9 mm settle near the wellbore, proppants with sizes of 0.6–1.4 mm are placed within the major fracture, and proppants with sizes of <0.5 mm can be carried to the far-end fracture and branched fracture. With an increase in sand carrier viscosity, the migration capability of proppants is improved significantly. When the sand carrier viscosity increases to 15 mPa s, proppants with sizes of 1.7–2.9 mm can be carried to the major fracture, and proppants with sizes of 0.6–1.4 mm can migrate to the far-end fracture and branched fracture. When the sand carrier viscosity increases to 25 mPa s, proppants with sizes of 1.7–2.9 mm can be placed uniformly in the near-wellbore zone and the major fracture, and proppants of other sizes do not settle significantly.

Self-generated proppants can be effectively carried by low-viscosity sand carrier and placed in stages. The proppant has good migration capability which changes, obviously, with sand carrier viscosity. In actual application, the sand carrier viscosity can be optimized according to the required placement position.

4.3. Pack permeability of solidified proppants

The pack permeability of three types of proppants under different closure stresses and at different temperatures are shown in Figs. 22 and 23.

Since the self-generated proppant has regular morphology (Fig. 24), its pack permeability is higher than quartz sand proppant, and close to the ceramsite proppant. As the closure stress increases, the accumulation morphology of quartz sand changes due to its irregular grain morphology, resulting in a significant decrease in permeability. When the closure stress increased to 35 MPa, the pack permeability of quartz sand decreased by 68%. This is due to proppant breaking under high closure stress. When the closure stress was 50 MPa, self-generated proppants and ceramsite proppants still maintained effective permeability. As the ambient temperature rose to 90 °C, the performance of the self-generated proppants can be maintained (Liu et al., 2020). This shows the self-generated proppant has good physical properties. It has regular

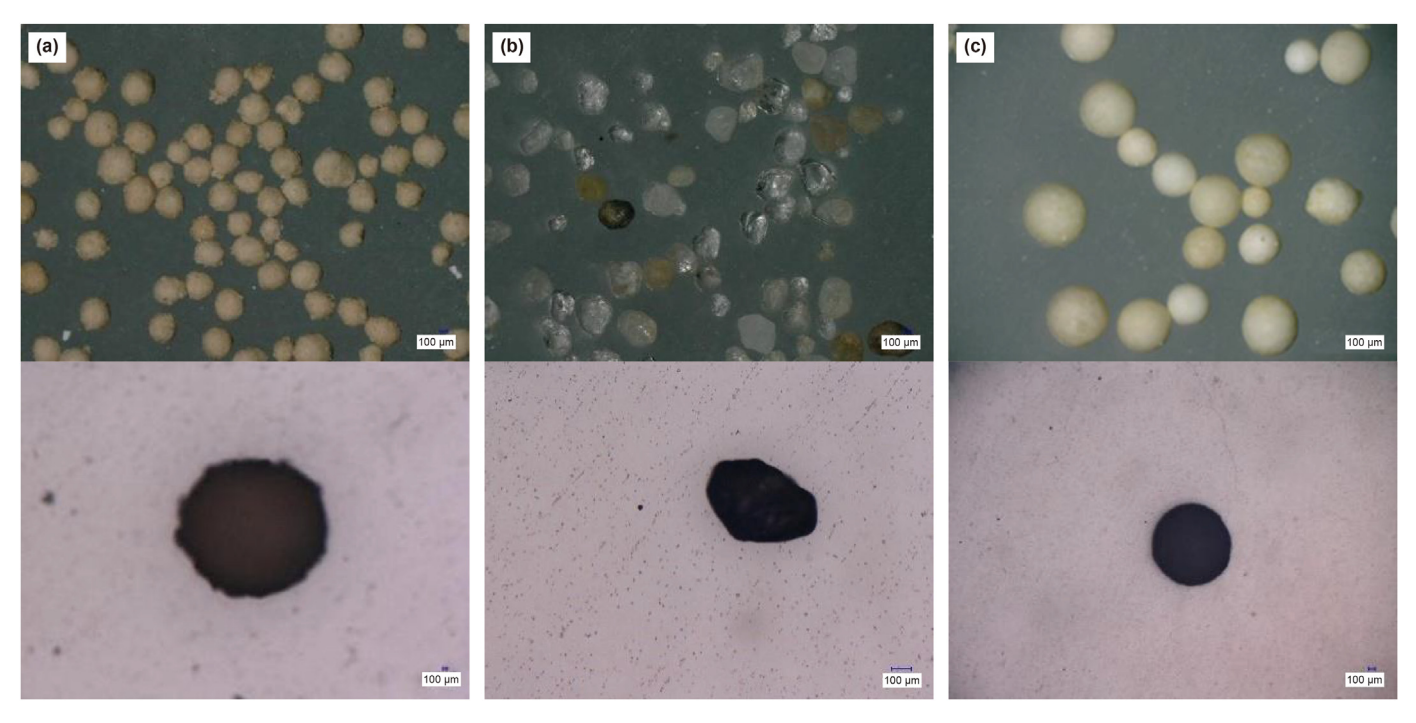


Fig. 24. Morphology of three types of proppants. (a) Ceramsite; (b) quartz sand; (c) self-generated proppants.

morphology and good temperature resistance, and its compressive strength is similar to that of the ceramsite proppant. These properties reflect the formation of efficient diversion channels after self-generated proppants are placed, and the generated proppants are applicable in reservoirs at high temperature and under high closure stress.

5. Conclusions

In this study, considering the unsatisfactory migration capability and placement effects of conventional solid proppants, a new type of self-generated proppants was developed by synthesizing and toughening a novel low-viscosity and low-density epoxy resin, and emulsifying the resin and its curing agent. The development and evaluation results for this novel self-generated proppant are as follows:

- (1) Low-viscosity and low-density epoxy resin was obtained when the product of thiol-ene click chemical reaction of eugenol and 1-thioglycerol reacts with the epichlorohydrin. The obtained epoxy resin, which had a viscosity of 686 mPa s and a density of 1.2 g/cm³ at 60 °C, and an epoxy value of 0.53 g/Eq, can meet proppant performance requirements.
- (2) The resin was toughened by adding graphite particles. When the graphite particle concentration was 3 wt%, the compressive strength of the resin increased from 50.8 to 72.1 MPa, and its toughness was also improved significantly. Analysis shows the mechanism of toughening the resin by graphite particles mainly includes the micro-cracking mechanism and crazing-nail anchor mechanism.
- (3) Hydrophilic SiO₂ nanoparticles was selected as the emulsifier in this study. The emulsification was carried out with the oilwater ratio of 1:6 by adding ethanol as diluent and stirring the solution at 300 rpm. Sizes of the obtained self-generated proppants include >2.9 mm (7 mesh), 1.7–2.8 mm (7/12 mesh), 0.85–1.4 mm (14/20 mesh), 0.6–0.710 mm (25/30 mesh), 0.25–0.5 mm (35/60 mesh) and <0.18 mm (80 mesh). The particles size distribution of the proppants can vary with the concentration of the emulsifier.
- (4) Self-generated proppants can be carried and transported by low-viscosity fracturing fluid and meet proppant placement requirements in different stages. Due to regular morphology, compressive strength, and temperature resistance, the selfgenerated proppants can form an effective percolation channel in a reservoir at high temperature and under high closure stress.

Acknowledgments

The authors would like to acknowledge the financial support of the National Natural Science Foundation of China (Grant No. 52074332) and express their gratitude to project ZR2020YQ36 supported by Shandong Provincial Science Fund for Excellent Young Scholars, the Major Scientific and Technological Projects of CNPC under Grand ZD 2019-184-002-003, and CNPC Innovation Found (Grant No. 2021DQ02-1006).

References

- Adnan, M., Sun, J., Ahmad, N., et al., 2021. Comparative CFD modeling of a bubbling bed using a Eulerian–Eulerian two-fluid model (TFM) and a Eulerian–Lagrangian dense discrete phase model (DDPM). Powder Technol. 383, 418–442. https://doi.org/10.1016/j.powtec.2021.01.063.
- Anton, N., Benoit, J.P., Saulnier, P., 2008. Design and production of nanoparticles formulated from nano-emulsion templates-a review. J. Contr. Release 128 (3), 185–199. https://doi.org/10.1016/j.jconrel.2008.02.007.

Chen, J.L., Chang, F.C., 2001. Temperature-dependent phase behavior in poly (epsilon-caprolactone) - epoxy blends. Polymer 42 (5), 2193–2199. https://doi.org/10.1016/S0032-3861(00)00511-5.

- Francis, B., Thomas, S., Asari, G.V., et al., 2006. Synthesis of hydroxyl-terminated poly (ether ether ketone) with pendent *tert*-butyl groups and its use as a toughener for epoxy resins. J. Polym. Sci. B Polym. Phys. 44 (3), 541–556. https://doi.org/10.1002/POLB.20713.
- Gaina, V., Gaina, C., 2009. New bismaleimide-epoxy resin system. Polym. Plast. Technol. Eng. 48 (5), 525–529. https://doi.org/10.1080/03602550902824325.
- Grishchuk, S., Karger-Kocsis, J., 2011. Hybrid thermosets from vinyl ester resin and acrylated epoxidized soybean oil (AESO). Express Polym. Lett. 5 (1), 2–11. https://doi.org/10.3144/expresspolymlett.2011.2.
- Groenzin, H., Mullins, O.C., 1999. Asphaltene molecular size and structure. J. Phys. Chem. 103, 11237–11245. https://doi.org/10.1021/jp992609w.
- Guo, L., Wang, L., Su, X., 2012. Research progress of new methods for toughening epoxy resin. Adv. Mater. Res. 490–495, 3598–3602. https://doi.org/10.4028/www.scientific.net/AMR.490-495.3598.
- Guo, T., Li, Y., Ding, Y., et al., 2017. Evaluation of acid fracturing treatment in shale formation. Energy Fuels 31 (10), 10479–10489. https://doi.org/10.1021/acs.energyfuels.7b01398.
- Guo, T., Wang, X., Li, Z., et al., 2018. Numerical simulation study on fracture propagation of zipper and synchronous fracturing in hydrogen energy development. Int. J. Hydrogen Energy 44 (11), 5270–5285. https://doi.org/10.1016/j.jijhydene.2018.08.072.
- Guo, T., Zhang, S., Wang, L., et al., 2012. Optimization of proppant size for frac-pack completion using new equipment. J. Petrol. Sci. Eng. 96–97, 1–9. https:// doi.org/10.1016/j.petrol.2012.08.007.
- Haaj, S.B., Thielemans, W., Magnin, A., et al., 2014. Starch nanocrystal stabilized Pickering emulsion polymerization for nanocomposites with improved performance. ACS Appl. Mater. Interfaces 6, 8263–8273. https://doi.org/10.1021/ am501077e
- Hu, X., Wu, K., Li, G., et al., 2018. Effect of proppant addition schedule on proppant distribution in a straight fracture for slickwater treatment. J. Petrol. Sci. Eng. 167, 110–119. https://doi.org/10.1016/j.petrol.2018.03.081.
- Jiang, H., Sun, L., Zhang, Y.R., et al., 2018. Estrogenic activity research of a novel fluorinated bisphenol and preparation of an epoxy resin as alternative to bisphenol A epoxy resin. Eur. Polym. J. 108, 507–516. https://doi.org/10.1016/ j.eurpolymj.2018.09.020.
- Jiang, J., Rui, Z., Hazlett, R., et al., 2019. An integrated technical-economic model for evaluating CO₂ enhanced oil recovery development. Appl. Energy 247, 190–211. https://doi.org/10.1016/j.apenergy.2019.04.025, 2019.
- Jin, F., Liu, H., Yang, B., et al., 2015. Synthesis and thermal properties of urethanecontaining epoxy resin. J. Ind. Eng. Chem. 24, 20–23. https://doi.org/10.1016/ i.iiec.2014.10.006.
- Kang, B., Jho, J.Y., Kim, J., et al., 2001. Effect of molecular weight between crosslinks on the fracture behavior of rubber-toughened epoxy adhesives. J. Appl. Polym. Sci. 79 (1), 38–48. https://doi.org/10.1002/1097-4628(20010103)79:1<38::AID-APP50>3.0.C0:2-0.
- Keller, A., Chong, H., Taylor, A.C., et al., 2017. Core-shell rubber nanoparticle reinforcement and processing of toughness fast-curing epoxy composites. Compos. Sci. Technol. 147. https://doi.org/10.1016/j.compscitech.2017.05.002, 78-88.
- Li, W., Zhao, X., Ji, Y., et al., 2016. Investigation of biodiesel-based drilling fluid, Part 1: biodiesel evaluation, invert-emulsion properties, and development of a novel emulsifier package. SPE J. 21 (5), 1755–1766. https://doi.org/10.2118/180918-PA.
- Liu, X., Qu, Z., Guo, T., et al., 2018. An innovative technology of directional propagation of hydraulic fracture guided by radial holes in fossil hydrogen energy development. Int. J. Hydrogen Energy 44 (11), 5286–5302. https://doi.org/10.1016/j.ijhydene.2018.07.189.
- Liu, X., Zhang, W., Qu, Z., et al., 2020. Feasibility evaluation of hydraulic fracturing in hydrate-bearing sediments based on analytic hierarchy processentropy method (AHPEM). J. Nat. Gas Sci. Eng. 81, 103434. https://doi.org/10.1016/ i.jngse.2020.103434.
- Luo, Z., Zhang, N., Zhao, L., et al., 2019. Thermoresponsive in situ generated proppant based on liquid—solid transition of a supramolecular self-propping fracturing fluid. Energy Fuels 33 (11), 10659—10666. https://doi.org/10.1021/ acs_energyfuels_9h02501
- Park, S.J., Jin, F.L., Lee, J.R., et al., 2005. Cationic polymerization and physicochemical properties of a bio-based epoxy resin initiated by thermally latent catalysts. Eur. Polym. J. 41 (2), 231–237. https://doi.org/10.1016/j.eurpolymj.2004.09.011.
- Pei, Y.X., Zhao, P.Q., Zhou, H.X., et al., 2021. Development and latest research advances of self-propping fracturing technology. SPE J. 26 (1), 281–292. https://doi.org/10.2118/202489-PA.
- Rao, R., Mondy, L., Sun, A., et al., 2002. A numerical and experimental study of batch sedimentation and viscous resuspension. Int. J. Numer. Methods Fluid. 39, 465–483. https://doi.org/10.1002/fld.246.
- Ritzenthaler, S., Court, F., David, L., et al., 2002. ABC triblock copolymers/epoxy-diamine blends. 1. Keys to achieve nanostructured thermosets. Macromolecules 35 (16), 6245–6254. https://doi.org/10.1021/ma0121868.
- Rui, Z., Guo, T., Feng, Q., et al., 2018. Influence of gravel on the propagation pattern of hydraulic fracture in the glutenite reservoir. J. Petrol. Sci. Eng. 165, 627–639. https://doi.org/10.1016/j.petrol.2018.02.067.
- Ren, Y., 2011. Research progress of toughening modification of epoxy resin. Thermosetting Resin 26 (3), 45–49. https://doi.org/10.13650/j.cnki.rgxsz.2011.03.011 (in Chinese).
- Wan, T., Zang, T., Zhang, R., et al., 2012. Cure behaviors and water up-take evaluation

of a new waterborne epoxy resin. J. Wuhan Univ. Technol.-Materials Sci. Ed. 27 (3), 437–442. https://doi.org/10.1007/s11595-012-0481-8.

- Wang, J., 2020. Experimental Study on the Formation of Proppant Particles in Situ. Ph.D. Dissertation. Xi'an Shiyou University. https://doi.org/10.27400/d.cnki.g-xasc.2020.000114 (in Chinese).
- Zhang, C., Zhao, L., Yu, D., et al., 2019. Evaluation on physical property and fracture conductivity of a new self-generating solid proppant. J. Petrol. Sci. Eng. 177 (2), 841–848. https://doi.org/10.1016/j.petrol.2019.03.013.
- Zhang, W., Qu, Z.Q., Guo, T.K., et al., 2019. Study of the enhanced geothermal system (EGS) heat mining from variably fractured hot dry rock under thermal stress. Renew. Energy 143, 855–871. https://doi.org/10.1016/j.renene.2019.05.054.
- Zhao, E., Hou, J., Du, Q., et al., 2021. Numerical modeling of gas production from methane hydrate deposits using low frequency electrical heating assisted depressurization method. Fuel 290, 120075. https://doi.org/10.1016/j.fuel.2020.120075.
- Zhao, L., Chen, Y., Du, J., et al., 2019. Experimental study on a new type of self-propping fracturing technology. Energy 183, 249–261. https://doi.org/10.1016/j.energy.2019.06.137.
- Zhou, W., Qi, S., Li, G., et al., 2005. Unsaturated polyester toughened with elastomers. Plastics 34 (1), 27–31. https://doi.org/10.3969/j.issn.1001-9456.2005.01.007 (in Chinese).